PAPER

Check for updates

An electrochemical sensor based on MWCNTs and a PCCN$_{222}$ peroxidase-like nanocomposite for sensitive and selective kaempferol detection

Yanna Ning,[a] Xianglei Li,[a] Guanghua Tong,[b] Feiyu Zhang,[b] Jun Hong [ID] *[b] and Baolin Xiao [ID] *[b]

Kaempferol (KA) is a flavonoid with a range of biological properties, including antitumor, antioxidant, antiviral and anti-inflammatory, and its extensive applications in biomedicine, food safety, and related fields underscore the importance of quantitative analysis for determining its concentration. In this study, an electrochemical sensor based on multi-walled carbon nanotubes (MWCNTs), PCN$_{222}$ and chitosan (CS) was developed for the determination of KA. MWCNTs exhibit hydrophobicity and conductivity, and they are better dispersed by DMF and crosslinked with PCN$_{222}$, which further improves the electrode's response, selectivity and sensitivity to KA due to the peroxide-like properties of PCN$_{222}$. The film formed by CS on the electrode surface serves to protect the nanocomposite from detaching during the operation. The linear range of this sensor is 0.01–0.4 and 0.6–9 μM, with a detection limit of 4.16 nM. This method can be used to detect the content of KA in plasma, which shows that the electrochemical sensor has strong practical application capabilities, as well as other advantages, such as high stability, strong anti-interference ability, and low detection limit. Moreover, the ultraviolet-visible spectrophotometer (UV) demonstrates that the catalytic rate of PCN$_{222}$ for KA is significantly faster than that for naringenin and puerarin. Therefore, the construction of CS/MWCNT–PCN$_{222}$/GCE electrochemical sensors has potential application value for clinical dosage control and monitoring of the drug metabolism of KA.

Introduction

Kaempferol (KA, 3,4′,5,7-tetrahydroxyflavone) is a flavonoid compound widely found in plant-derived foods and traditional medicinal plants.[1] KA is a strong natural antioxidant with several biological properties, including antiviral, anti-inflammatory, antidiabetic, antioxidant, and anticancer properties, and therefore has a wide range of potential applications in the treatment and prevention of diabetic complications and atherosclerosis,[2–11] as well as in reducing neurological and cardiac damage, which will provide valuable references for future research and development of medicines. Due to its rich biological activities, KA has been extensively utilized in clinical practice. However, excessive intake may cause adverse effects,[12–14] so developing a sensitive assay for KA is important for pharmacodynamic studies, assessing the safety of clinical drug use and monitoring drug metabolism.

Numerous techniques, including high performance liquid chromatography[15] and ultraviolet-visible spectrophotometer (UV),[16] capillary electrophoresis[17] and electrochemical methods[18] have been reported for the quantitative determination of KA. In contrast to the aforementioned techniques, electrochemical methods stand out due to their unique capability to scrutinize the electrochemical behavior of flavonoids at the electrode surface, enabling swift and microscale analysis of biological samples. Moreover, they are celebrated for their rapid response, exceptional sensitivity, and cost effectiveness. In recent years, electrochemical methods have garnered significant attention for KA detection. For example, Liang *et al.*[19] prepared a simple and sensitive multi walled carbon paste electrode sensor using cetyltrimethylammonium bromide carboxyl multi walled carbon nanotubes (CTAB-MWCNTs) and successfully used it to determine the content of KA and quercetin in several plants. The MIL-100(Fe)-multi walled carbon nanotube/poly (3,4-ethylenedioxythiophene) (MIL-100(Fe)-MWCNTs/PEDOT) modified glassy carbon electrode constructed by Zhang *et al.*[20] was used to detect the content of KA in Xindakang tablets. Tan *et al.*[21] introduced β-cyclodextrin/fullerene graphene oxide/nickel metal organic framework (β-CD/C60-GO/Ni-MOF) nanocomposites on electrodes for the detection of KA. These sensors are of the non-enzymatic electrochemical type, yet they have limited selectivity. However, despite their merits, these non-enzymatic electrochemical sensors are marred by limited selectivity. Given that selectivity

[a]Department of Medical Laboratory, Kaifeng Central Hospital, Kaifeng 475000, China
[b]School of Life Sciences, Henan University, Kaifeng 475000, China. E-mail: hongjun@henu.edu.cn; xiaobaolin@henu.edu.cn

is the cornerstone of sensor practicality, our research focuses on constructing a nano-enzymatic electrochemical sensor to augment KA selectivity.

Nanozymes, particularly those possessing peroxidase activity, have been extensively applied in the field of electrochemical sensors.[22] In contrast to natural enzymes, nano-enzymes boast the benefits of being cost effective and having an easy preparation process, easy modification, and good stability.[23] Metal–organic frameworks (MOFs), which are highly crystalline network complexes constructed from metal ions or clusters linked by organic ligands, represent a typical class of nanoenzymes. Their burgeoning popularity stems from their peroxidase-like activity, tunable structure, environmental adaptability, high porosity, expansive specific surface area, and abundant surface active sites.[24–28] MOFs have permeated diverse industrial sectors, including gas separation, catalysis, energy storage, medicine delivery, and electrochemical sensors.[29–33] Zr-MOF has garnered substantial attention.[34] PCN_{222} (also known as MOF-545) is a Zr-based MOF that has been the focus of research over the past decade. It exhibits exceptional chemical and thermal stability, with a high coordination number and a large ionic radius Zr metal center. This unique composition allows it to form versatile structures by integrating multiple organic ligands, thereby broadening its applicability. Moreover, its nanochannels are particularly suitable for doping and modification of nano-materials.[33,35] In this study, PCN_{222} is modeled as a nano-enzyme to achieve an electrochemical sensor for KA using the unique properties of multi-walled carbon nanotubes (MWCNTs, thermal, electrical, mechanical, etc.).[36,37]

Considering the aforementioned factors, we constructed an electrochemical sensor based on MWCNTs and a $PCCN_{222}$ peroxidase-like nanocomposite for KA detection (Fig. 1). PCN_{222} is used as a nano-enzyme to catalyze KA, which enhances the selectivity of the electrode. The dispersion of MWCNTs is improved by the addition of DMF, which ensures that distribution is achieved uniformly on the electrode surface, thereby enhancing the sensor performance. Given that different phenolic compounds have different oxidation potentials and are recognized differently by PCN_{222}, we demonstrated the strong selectivity of PCN_{222} for KA under UV irradiation. Under the same conditions, we determine whether $PCCN_{222}$ could catalyze them by observing changes in the absorbance of

characteristic peaks. The materials were characterized and examined using scanning electron microscopy (SEM) and an Energy Dispersive Spectrometer (EDS). The constructed sensor efficiently measures the amount of KA in mouse plasma and has the benefits of speed, sensitivity, and remarkable selectivity.

Experimental section

Reagents and materials

KA, naringenin, and puerarin were purchased from Shanghai Aladdin Biochemical Technology Co., Ltd. Glucose (Glu, ≥99%), sodium dihydrogen phosphate ($NaH_2PO_4 \cdot 2H_2O$, ≥99%), and disodium phosphate ($Na_2HPO_4 \cdot 12H_2O$, ≥ 99.0%) are sourced from Sigma Aldrich (St. Louis, Missouri, USA). Vitamin B1, Vitamin C, and urea were procured from Beijing Dingguo Biotechnology Co., Ltd., Beijing Aoboxing Biotechnology Co., Ltd., and China National Pharmaceutical Group Chemical Reagent Co., Ltd., respectively. Potassium chloride (KCl) and sodium chloride (NaCl) were purchased from Tianjin DeEn Chemical Reagent Co., Ltd. Zirconium-based porphyrin metal organic framework (PCN_{222}) and multi-walled carbon nanotubes (MWCNTs) were obtained from Jiangsu Xianfeng Nanomaterials Technology Co., Ltd. N,N-Dimethylformamide (DMF) were purchased from Chengdu Yirui Biotechnology Co., Ltd. Chitosan (CS) was obtained from Biotechnology Co., Ltd.

Apparatus

The CHI660E electrochemical workstation was utilized for all electrochemical measurements (CHI Instrument, Austin, TX, USA). The experiment was conducted at 25 °C using a three-electrode (working electrode, saturated Ag/AgCl electrode, and platinum wire as reference electrodes). Differential pulse polarography voltammetry (DPV) and cyclic voltammetry (CV) were performed in a 50 mM pH 5 phosphate buffer solution (PBS). The testing conditions for CV were a scanning rate of $0.1\ V\ s^{-1}$ and a standing time of 2 s, while the testing conditions for DPV were a potential increment of 0.04 V, an amplitude of 0.025 V, an amplitude of 15 Hz, and a standing time of 2 s. Electrochemical impedance spectroscopy (EIS) was carried out in a 0.1 M KCl solution containing 5 mM $[Fe\ (CN)_6]^{3-/4-}$, with a frequency range of 10^2–10^6 Hz. Field emission scanning electron microscope (JEOL JSM-7610F Plus, Japan Electronics Corporation) was used for morphological characterization of nanocomposites at 5 kV, while high-speed centrifuge (TGL-16G, Shanghai Anting Scientific Instrument Factory) was used to centrifuge blood samples at 3000 rpm for 10 minutes. A spectral study of PCN_{222}-catalyzed KA was conducted using a UV visible spectrophotometer (Evolution 220, Thermo, Shanghai, China). 2.5 mM KA, puerarin and naringenin were added to the 3000 μL system with PCN_{222} and H_2O_2 (1 mM), respectively. HRP catalyzes KA, naringenin and puerarin at the same concentrations as mentioned above. Continuous spectral scanning at 220–700 nm was performed using a UV spectrophotometer for the HRP-catalyzed KA-H_2O_2 system and PCN_{222}-catalyzed KA-H_2O_2 system.
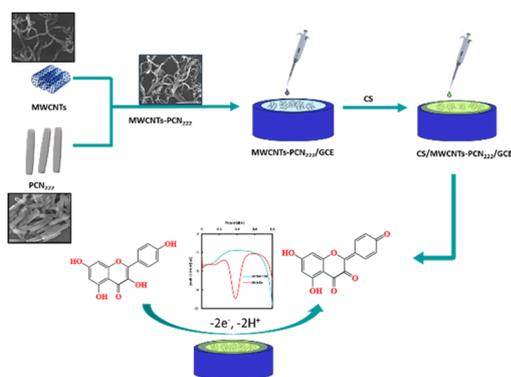

Fig. 1 Preparation scheme of CS/MWCNT−PCN_{222}/GCE.

Preparation of modified electrodes

Accurately weighed MWCNTs and PCN_{222} were prepared into a 2 mg mL^{-1} dispersion using DMF and ultrapure water, respectively. After 20 minutes of ultrasonic treatment, the two were mixed in a 1:1 (v/v) volume ratio to obtain MWCNT–PCN_{222} nanocomposites. According to previous studies,[38] first, the surface of a GCE with a diameter of 3.0 mm was polished to a mirror finish using 0.3 and 0.05 μm alumina powders. Next, the polished electrodes were placed in double distilled water and 75% ethanol for ultrasonic treatment for 15 minutes. Then, they were dried and placed in a drying tower for later use. 5 μL of MWCNT–PCN_{222} mixed liquid droplets were added to the glassy carbon electrode (GCE) surface to obtain MWCNT–PCN_{222}/GCE. Finally, 2.5 μL of CS was dropped onto the modified composite film (Fig. 1), and the sample was placed in a drying tower to air dry naturally, resulting in CS/MWCNT–PCN_{222}/GCE.

Preparation of actual sample

The actual sample preparation procedure is outlined below. The rat blood sample was taken by applying the orbital vein puncture method.[39] A certain amount of blood was extracted from the mouse eye socket, transferred to a heparin sodium anticoagulant tube, and then transferred to a centrifuge tube and centrifuged at 3000 rpm for 10 minutes. After separating the plasma, a known amount of KA solution was added to the plasma.

Results and discussion

Characterization of modified materials

SEM was used to observe the morphology of MWCNTs (a), DMF-MWCNTs (b), PCN_{222} (c), MWCNT–PCN_{222} (d and e), and CS-MWCNT–PCN_{222} (f) in the SEM images at 5 kV. It is the EDS spectrum of MWCNT–PCN_{222} nanocomposite (g).

SEM pictures of several modified materials are displayed in Fig. 2 MWCNTs appear as hollow tubular structures with a diameter of approximately 10–20 nm, as shown in Fig. 2a. When MWCNTs are used alone to modify the electrode, they tend to aggregate into clusters with each other. The addition of DMF helps to improve the dispersibility of MWCNTs (Fig. 2b). Fig. 2c shows the microstructure of PCN_{222}. The SEM image shows that PCN_{222} is a nano rod-like structure with a diameter of about 100 nm, a length of about 300 nm, and uniform distribution, which is consistent with literature reports.[40] Fig. 2d and e show SEM images of MWCNT–PCN_{222} composite material at different magnifications. The even distribution of PCN_{222} on the MWCNT surface confirms the successful preparation of the MWCNT–PCN_{222} composite material. The presence of the Zr element in the EDS spectrum of Fig. 2g further corroborates the formation of MWCNT–PCN_{222} nanocomposites. Fig. 2f shows that CS covers the surface of MWCNT–PCN_{222} composite material to form a thin film, indicating the successful preparation of CS/MWCNT–PCN_{222} nanocomposite material.

EIS is a fundamental technique for describing electron transfer behavior on the surface of composite material-
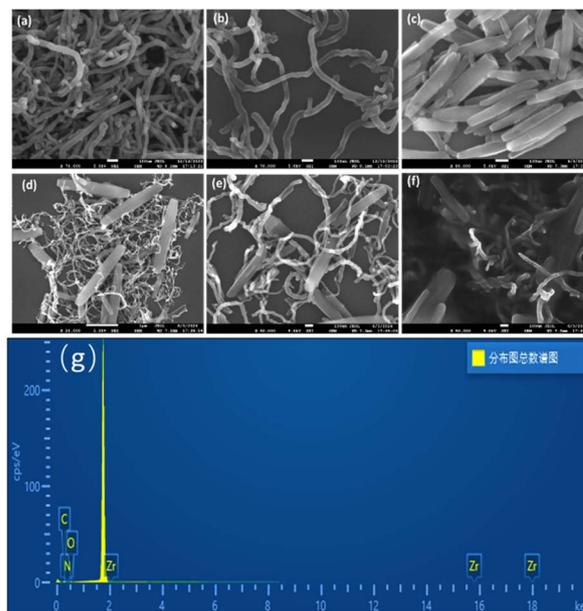

Fig. 2 SEM images of MWCNTs (a), DMF-MWCNTs (b), PCN_{222} (c), MWCNT–PCN_{222} (d and e), and CS-MWCNT–PCN_{222} (f) at 5 kV, and EDS spectrum of MWCNT–PCN_{222} nanocomposite material (g).

modified electrodes.[17] The impedance values were fitted using the Randles equivalent circuit model (illustrated in Fig. 3), which includes a double-layer capacitor (C_{dl}), a solution resistance (R_s), a charge transfer resistance (R_{ct}), and a diffusion resistance (Z_w).[17] From Fig. 3, it can be observed that EIS consists of a semi-circular part and a straight line part. The straight line portion of the low-frequency region reflects diffusion-controlled mass transfer limitations (Warburg impedance), suggesting that the redox process is limited at this stage by the rate of diffusion of the analyte to the electrode surface. The diameter of each semicircle corresponds to the electron transfer resistance on its electrode surface. As the semicircle diameter grows, the electron transfer resistance grows, making surface electron migration more challenging.[41] The radius of the semicircle in Fig. 3 decreases in the following
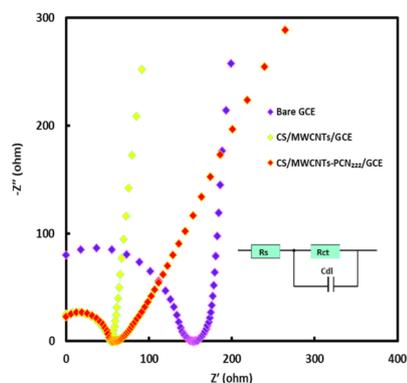

Fig. 3 EIS of bare GCE, CS/MWCNTs/GCE, and CS/MWCNT–PCN_{222}/GCE in 0.1 M KCl solution containing 5 mM $[Fe(CN)_6]^{3-/4-}$. (Illustration: Randles equivalent circuit).

order: Bare GCE > CS/MWCNT/GCE > CS/MWCNT–PCN$_{222}$/GCE. The bare GCE exhibits the largest semicircle with the highest electron transfer resistance (R_{et} = 216 Ω). After adding MWCNTs to bare GCE, the semicircle's diameter dramatically shrank, and the R_{et} decreased to 94 Ω, indicating that the addition of carbon nanomaterials enhanced electron transfer on the electrode surface and improved electrode conductivity. When GCE was modified with MWCNT-PCN$_{222}$ nanocomposite material, the R et decreases to 77.68 Ω, which can be explained by the internal jump mechanism of PCN$_{222}$ to improve electron mobility.[42] The high specific surface areas of MWCNTs and PCN$_{222}$ greatly enhance the conductivity and electrochemical activity of the sensing electrode. In addition, the synergistic effect of MWCNT-PCN$_{222}$ nanocomposite enables efficient electrocatalysis of the target analyte. Based on the above data, CS/MWCNT–PCN$_{222}$ was successfully immobilized on the surface of GCE.

Electrochemical behavior of KA on nanocomposite-modified electrodes

The electrochemical response of 5.0 μM KA on different modified electrodes in 50 mM, pH 5.0 PBS was studied using CV. As shown in Fig. 4a, compared with the weak oxidation peak current response on the bare electrode (curve a′), the CS/MWCNT/GCE (curve b′) exhibits a more pronounced oxidation peak. The oxidation peak of CS/MWCNT–PCN$_{222}$/GCE (curve c′) is even clearer and more prominent. Specifically, the oxidation peak current of CS/MWCNT–PCN$_{222}$/GCE is 3.5 times that of CS/MWCNT/GCE, indicating that the CS/MWCNT–PCN$_{222}$/GCE electrode has superior electrocatalytic activity for KA. The increase in the oxidation peak current mainly depends on the synergistic promotion of MWCNT–PCN$_{222}$ on the adsorption and charge transfer of analytes on the electrode surface.[43] In addition, the high-density catalytic adsorption sites provided by the electroactive centers of MOF structures on the sensor surface, as well as the high specific surface area of MWCNT–PCN$_{222}$ nanocomposites, further facilitate electron transfer on the electrode surface.
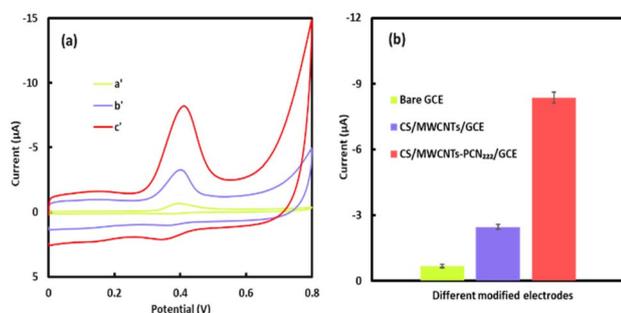
Effect of scan rate

To further investigate the reaction process of KA on the CS/MWCNT–PCN$_{222}$/GCE surface, the impact of scan rates spanning from 10 to 1000 mV s^{-1} on electron transfer at the electrode surface was examined. Fig. 5a shows the cyclic voltammetry response of KA at different scan rates on CS/MWCNT–PCN$_{222}$/GCE. It can be observed that as the scanning rate increases, the oxidation peak potential (E_{pa}) experiences a positive shift, and the oxidation peak current (I_{pa}) exhibits linear growth in the range of 10–500 mV s^{-1} (as shown in Fig. 5b). The linear regression equations are I_{pa} (μA) = −53.0013 v (V s^{-1})-2.5804 (R^2 = 0.9950) and I_{pc} (μA) = 55.4953 v (V s^{-1}) + 1.8932 (R^2 = 0.9986), indicating that the redox process of KA on the CS/MWCNT–PCN$_{222}$/GCE surface is an adsorption-controlled process, which is in accordance with earlier reported results.[44]

In addition, the linear relationship between the oxidation potential (E_{pa}) of KA and the natural logarithm of the scanning rate (ln v) is shown in Fig. 5c, and the relevant linear regression equation is E_{pa} (V) = 0.0248 ln v + 0.2042 (R^2 = 0.9963). Based on Laviron's theory, we have

$$E_{pa} = E^{\circ\prime} + \frac{RT}{\alpha nF} \ln \frac{RTk_s}{\alpha nF} + \ln v, \quad (1)$$

where $E^{\circ\prime}$ is the formal potential, n denotes the number of electrons transferred, v represents the scan rate, k_s denotes the apparent rate constant for electron transfer, and F and R denote the Faraday constant and the gas constant, respectively. Additionally, T denotes the temperature. In the context of the electrooxidation process of KA on the electrode, the value of αn can
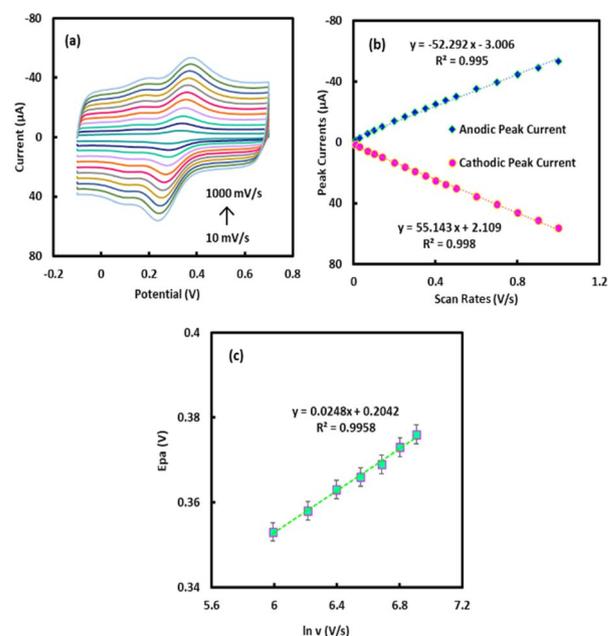

Fig. 4 (a) CVs of different modified GCEs in 50 mM pH 5 PBS containing 5 μM KA at a scan rate of 100 mV s^{-1} (where a′, b′, and c′ are bare GCE, CS/MWCNTs/GCE, and CS/MWCNT–PCN$_{222}$/GCE, respectively). (b) Oxidation peak current of different modified electrodes in 10 μM KA.

Fig. 5 (a) CVs of CS/MWCNT–PCN$_{222}$/GCE to 5 μM KA at different scan speeds in PBS at 50 mM pH 5.0. (b) Relationship between peak current and scanning speed. (c) Linear relationship between oxidation peak potential E_{pa} and ln v.
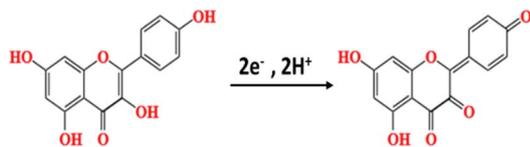
Fig. 6 Electrochemical reaction mechanism of KA.

be calculated as 1.04 using eqn (1). Generally speaking, the value of α in irreversible electrochemical processes is about 0.4–0.6,[45] so $\alpha = 0.52$ and $n = 2$. Therefore, the number of electrons involved in the redox reaction of KA on CS/MWCNT–PCN$_{222}$/GCE is 2, and its electrochemical reaction mechanism is illustrated in Fig. 6, aligning with previous studies.[44]

Effect of pH value

The pH value of the buffer will affect the electrochemical behavior of KA on CS/MWCNT–PCN$_{222}$/GCE. The electrochemical behavior of 5 μM KA was investigated in a pH range of 3.0–9.0 utilizing a 50 mM PBS solution as the supporting electrolyte (Fig. 7a). When the pH value of the buffer ranged from 3.0 to 9.0, the oxidation peak current first increased and then gradually decreased. The maximum oxidation peak current for KA was achieved in PBS with pH 5.0 (Fig. 7b). Therefore, PBS with pH 5.0 was selected as the optimal pH for the supporting electrolyte for subsequent experiments. As the pH value of the buffer solution increases, the oxidation peak potential shifts towards the negative direction, indicating the involvement of protons in the reaction.[44] The oxidation peak potential (E_{pa})

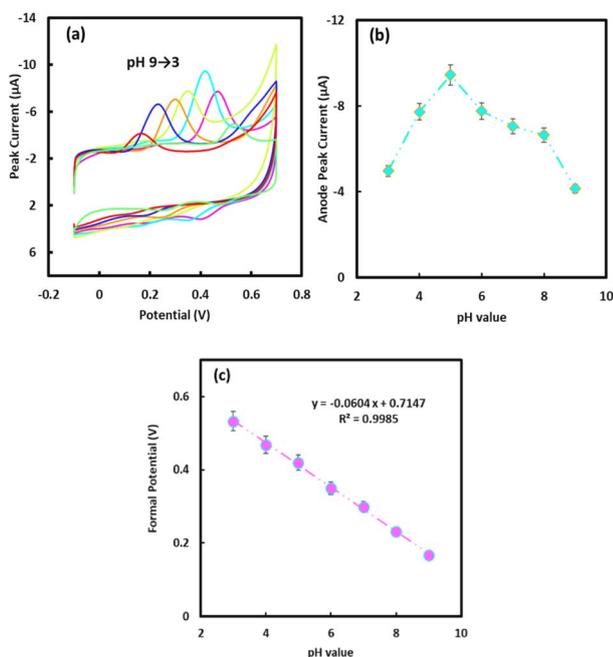exhibits a linear correlation with the solution's pH value (Fig. 7c), which is represented by the linear regression equation: $E_{pa} = -0.0604$ PH $+ 0.7147$ ($R^2 = 0.9985$). The slope of the equation is -60.4 mV pH^{-1}, which is close to the Nernst theory value of -59.2 mV pH^{-1}.[38] This indicates that KA participates in the oxidation process on CS/MWCNT–PCN$_{222}$/GCE in the form of isoquanta and isoquanta. Based on the study of scanning speed, the number of electrons involved in the oxidation–reduction reaction of KA on CS/MWCNT–PCN$_{222}$/GCE is 2. It can be concluded that the oxidation reaction process of KA on the electrode surface is a double electron and double proton reaction.

Measurement of KA concentration

In this study, the DPV technique was employed to quantitatively analyze KA (Fig. 8). It was observed that the oxidation peak current increased as the concentration of KA increased, exhibiting two distinct linear segments correlating the oxidation peak current with the KA concentration. The linear equation in the concentration scope of 0.01–0.4 μM is I_{pa} (μA) $= 6.3087c$ (μM) $+ 1.7354$ ($R^2 = 0.9927$). The linear equation in the concentration range of 0.6–9.0 is I_{pa} (μA) $= 0.4127$ c (μM) $+ 4.7491$ ($R^2 = 0.9922$). According to formula (2), the detection limit LOD of 4.16×10^{-3} μM is calculated as follows:[46]

$$\text{LOD} = 3 \times S/q, \qquad (2)$$

where S denotes the standard deviation of the intercept and q denotes the slope of the calibration graph. Table 1 summarizes the previously reported methods and related parameters for detecting KA. Relative to previous studies,[17,20,46,47] the preparation process of GCE modified with CS/MWCNT–PCN$_{222}$ nanocomposite material is simple, with enhanced sensitivity and lower detection limit for KA.

Reproducibility, stability, and storage stability

The determination of flavonoids is influenced by multiple factors, among which repeatability is crucial. Therefore, under the most suitable experimental conditions, five electrodes CS/MWCNT–PCN$_{222}$/GCE with the same modification were

Fig. 7 (a) Effects of pH value the CVs of CS/MWCNT–PCN$_{222}$/GCE in 50 mM PBS 5 μM KA at a scan rate of 100 mV s^{-1}. (b) Relationship between pH value and oxidation peak current. (c) Linear relationship between peak oxidation potential E_{pa} and buffer pH.
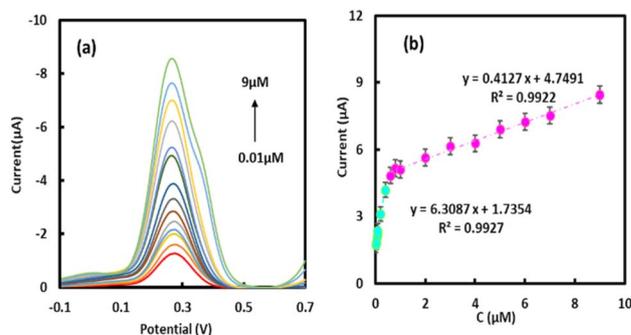

Fig. 8 (a) DPV response of CS/MWCNT–PCN$_{222}$/GCE to different concentrations of KA. (b) Relationship between peak oxidation current and concentration of of KA.

Table 1 Comparison of analytical performance of different KA sensors[a]

Electrode	Liner range (μM)	LOD (μM)	Method	Sensitivity (μA μM^{-1})	Reference
PVP/CPE	0.05–0.50	0.04	SWV	10.75	47
pn-MWCNTs/GCE	0.05–4.55	0.05	DPV	0.019	46
β-CD/Ni-MOF/C$_{60}$-GO/GCE	20–50	0.058	DPV	0.039	21
MIL-100(Fe)-MWCNTs/PEDOT/GCE	0.05–1.95	0.0132	DPV	17.8	20
A-ZnWO$_4$/C/GCE	0.009–0.7	0.002	DPV	—	48
CS/MWCNT–PCN$_{222}$/GCE	0.01–0.4	0.004	DPV	6.31	This work

[a] Abbreviation: PVP: olyvinylpyrrolidone; CPE: carbon paste electrode; pn-MWCNTs: NH$_3$-plasma treated MWCNTs, β-CD: β-cyclodextrin; Ni-MOF: nickel-based metal organic framework; C60-GO: fullerene graphene oxide composite material; PEDOT: poly 3,4-ethylenedioxythiophene; A-ZnWO$_4$/ C: acidized zinc tungstate/porous nanocarbon composite material.

prepared. The relative standard deviation (RSD) of the response to 1 μM KA was 4.8%, indicating the good reproducibility of the electrochemical sensor (Fig. 9a). For the same CS/MWCNT–PCN$_{222}$/GCE modified electrode, the continuous response to 5 μM KA was tested, and the oxidation peak current exhibited an RSD of 1.7% (Fig. 9b). In addition, after keeping the modified electrode at 4 °C for 28 days, the electrochemical response to KA was remeasured, with the oxidation peak current decreasing by less than 10%. The above results indicate that the CS/MWCNT–PCN$_{222}$ modified electrode has good repeatability and stability for KA determination.

Anti interference capability

The anti-interference performance of the constructed electrode for KA is shown in Fig. 10. The UV scanning spectra of the catalytic reaction processes of systems a (KA-H$_2$O$_2$), b (naringenin-H$_2$O$_2$), and c (puerarin-H$_2$O$_2$) in the presence of PCN$_{222}$

(exhibit Soret bands at 420 nm)[49] are shown in Fig. 10a–c, respectively. Continuous scanning of the UV spectra at a certain time interval show that compared with systems b and c, the UV
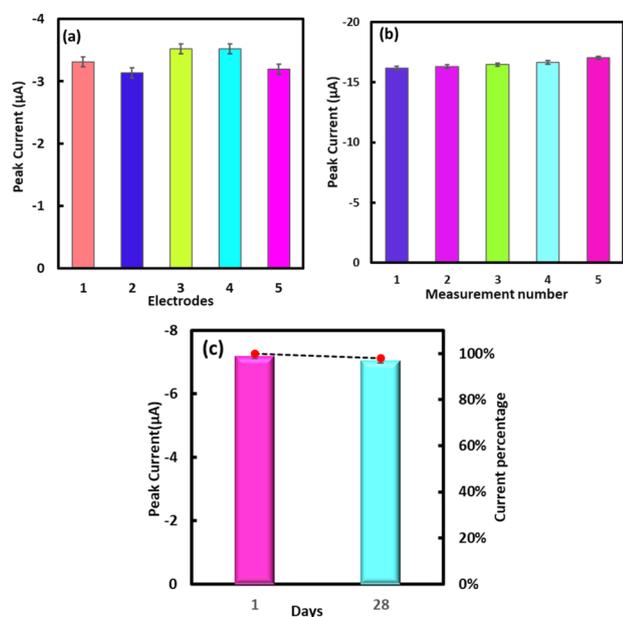

Fig. 10 UV spectra of continuous scanning (a) PCN$_{222}$-KA-H$_2$O$_2$, (b) PCN$_{222}$-puerarin-H$_2$O$_2$ and (c) PCN$_{222}$-naringenin-H$_2$O$_2$. (d) ΔA versus time in 50 mM pH 5 PBS containing PCN$_{222}$, H$_2$O$_2$, and different flavonoids (KA, puerarin and naringenin). (Illustration: (a) HRP-KA-H$_2$O$_2$, (b) HRP-puerarin-H$_2$O$_2$ and (c) HRP-naringenin-H$_2$O$_2$.) (d) ΔA versus time in 50 mM pH 5 PBS containing PCN$_{222}$, H$_2$O$_2$, and different flavonoids (KA, puerarin and naringenin). (e) Anti-interference ability of CS/MWCNT–PCN$_{222}$/GCE in 50 mM pH 5 PBS containing 50 μM different interfering substances (Glu, UA, Vb1, AA, KCl, and NaCl), 2 μM flavonoids interfering substances (puerarin and naringenin) and 2 μM KA (pink).

Fig. 9 (a) Response of five independent electrodes prepared in 50 mM, pH 5.0 PBS to the oxidation peak current of 1 μM KA. (b) DPV response of the same modified electrode to 5 μM KA. (c) Storage stability of the CS/MWCNT–PCN$_{222}$/GCE.
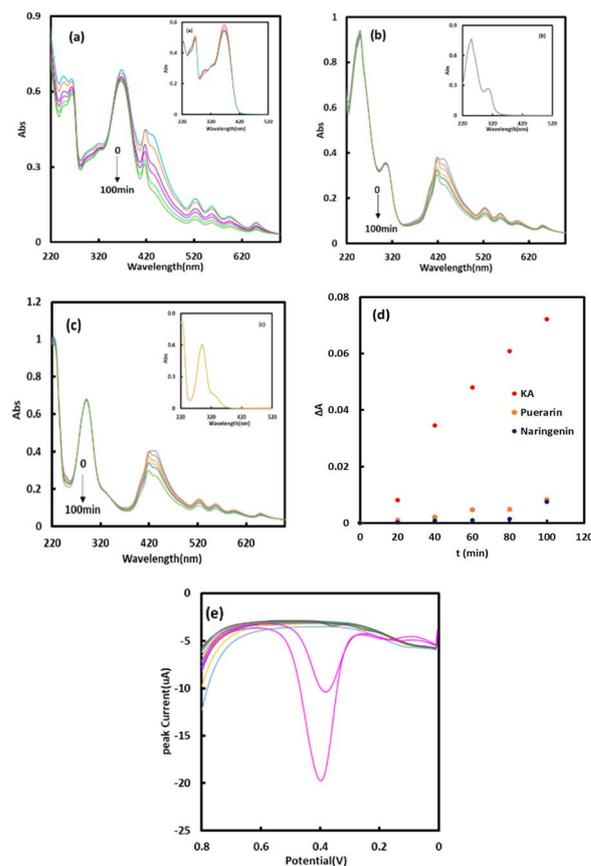
Table 2 Detection of KA content in rat plasma samples ($n = 3$)

Samples	Add (μM)	Found (μM)	Recovery%	RSD%
Rat serum	0.05	0.049	98.8	4.1
	0.10	0.105	105.1	4.7
	1.0	1.024	102.3	3.9
	2.5	2.441	98.0	1.6

absorption peak of system a (KA-H$_2$O$_2$) continuously decreased under the promotion of PCN$_{222}$, and the reaction rate was higher at 368 nm. From Fig. 10d, it can be observed that PCN$_{222}$ has the fastest catalytic rate for KA, which may lead to some flavonoids (such as naringenin and puerarin) with high anti-interference performance. These results are consistent with the results obtained from the reaction process of system a (KA-H$_2$O$_2$) in the presence of HRP, as shown in Fig. 10. These findings confirm the peroxidase-like activity of PCN$_{222}$, demonstrating its rapid KA catalytic rate, powerful anti-interference capacity, and high selectivity.

Good selectivity is one of the important factors determining the practical application of sensors.[50] Therefore, under the most suitable experimental conditions, the DPV method was used to add 50 mM potassium chloride (KCl), glucose (Glu), NaCl, vitamin B1 (Vb1), ascorbic acid (AA), uric acid (UA), 2 mM naringenin, puerarin, and two doses of KA to verify the anti-interference ability of the electrochemical sensor against potential interfering substances in biological samples for KA detection.[51] As depicted in Fig. 10e, the present response of 2 μM KA is markedly greater than that observed with interfering substances, demonstrating that CS/MWCNT–PCN$_{222}$/GCE exhibits strong selectivity and resistance to interference.

Actual sample measurement

To assess the practicality of this approach, the standard addition technique was employed to evaluate the spiked recovery rate of KA in rat plasma samples (Table 2). The recovery rates ranged from 98.0% to 105.1%, suggesting that this method is effectively suited for detecting KA resveratrol in complex biological samples.

Conclusion

A nano enzyme electrochemical sensor was constructed based on CS/MWCNT–PCN$_{222}$ nanomaterial-modified glassy carbon electrode for detecting the flavonoid compound KA. PCN$_{222}$ with peroxidase-like properties contributes to the selectivity and sensitivity of electrochemical sensors. In addition, this electrochemical sensor demonstrates stability and excellent reproducibility for KA detection, enabling the accurate measurement of KA levels in real biological samples. The good recovery rate indicates its potential application value in actual blood drug concentration detection.

Ethical statement

All animal-related procedures were performed in accordance with the Guidelines for Care and Use of Laboratory Animals of Henan University and approved by the Animal Ethics Committee of Henan University (HUSOM2021-198).

Data availability

The data generated or used in this study are included in the submitted article. Additional data used for the study are available from the corresponding authors upon reasonable request.

Author contributions

Yan-Na Ning, Xiang-Lei Li and Guang-Hua Tong: formal analysis, visualization, investigation, data curation, and writing—original draft. Fei-Yu Zhang: formal analysis, investigation, and data curation. Jun Hong and Bao-lin Xiao: conceptualization, methodology, resources, supervision, and writing—review and editing. All authors have read and agreed to the published version of the manuscript.

Conflicts of interest

The authors declare no conflicts of interest.

Acknowledgements

References

1 H. R. Nejabati and L. Roshangar, *J. Food Biochem.*, 2022, **46**, e14375.

2 J. Chen, H. Zhong, Z. Huang, X. Chen, J. You and T. Zou, *Antioxidants*, 2023, **12**, 1642.

3 F. Alrumaihi, S. A. Almatroodi, H. O. A. Alharbi, W. M. Alwanian, F. A. Alharbi, A. Almatroudi and A. H. Rahmani, *Molecules*, 2024, **29**, 2007.

4 E. Amjad, B. Sokouti and S. Asnaashari, *Cancer Cell Int.*, 2022, **22**, 260.

5 Y. Kamisah, J. Jalil, N. M. Yunos and S. Zainalabidin, *Plants*, 2023, **12**, 2096.

6 J. Wang, J. Mao, R. Wang, S. Li, B. Wu and Y. Yuan, *Front. Pharmacol*, 2020, **11**, 424.

7 M. M. Rahman, M. S. Rahaman, M. R. Islam, F. Rahman, F. M. Mithi, T. Alqahtani, M. A. Almikhlafi, S. Q. Alghamdi, A. S. Alruwaili, M. S. Hossain, M. Ahmed, R. Das, T. B. Emran and M. S. Uddin, *Molecules*, 2022, **27**, 233.

8 P. Xue, X. You, L. Ren, W. Yue and Z. Ma, *Arch. Biochem. Biophys.*, 2024, **761**, 110154.

9 A. Periferakis, A. T. Periferakis, L. Troumpata, K. Periferakis, A.-E. Scheau, I. Savulescu-Fiedler, A. Caruntu, I. A. Badarau, C. Caruntu and C. Scheau, *Int. J. Mol. Sci.*, 2023, **24**, 16299.

10 A. Periferakis, K. Periferakis, I. A. Badarau, E. M. Petran, D. C. Popa, A. Caruntu, R. S. Costache, C. Scheau, C. Caruntu and D. O. Costache, *Int. J. Mol. Sci.*, 2022, **23**, 15054.

11 H. Song, J. Bao, Y. Wei, Y. Chen, X. Mao, J. Li, Z. Yang and Y. Xue, *Oncol. Rep.*, 2015, **33**, 868–874.

12 A. Engen, J. Maeda, D. E. Wozniak, C. A. Brents, J. J. Bell, M. Uesaka, Y. Aizawa and T. A. Kato, *Mutat. Res.*, 2015, **784–785**, 15–22.

13 M. Ezzati, B. Yousefi, K. Velaei and A. Safa, *Life Sci.*, 2020, **248**, 117463.

14 G. Galati and P. J. O'Brien, *Free Radical Biol. Med.*, 2004, **37**, 287–303.

15 C. D. Stalikas, *J. Sep. Sci.*, 2007, **30**, 3268–3295.

16 H. Jiang, U. H. Engelhardt, C. Thräne, B. Maiwald and J. Stark, *Food Chem.*, 2015, **183**, 30–35.

17 F. Gatea, E. D. Teodor, A. O. Matei, G. I. Badea and G. L. Radu, *Food Anal. Methods*, 2015, **8**, 1197–1206.

18 S. George Ashlay, R. Rajeev, D. A. Thadathil and A. Varghese, *Crit. Rev. Anal. Chem.*, 2023, **53**, 1133–1173.

19 Z. Liang, H. Zhai, Z. Chen, S. Wang, H. Wang and S. Wang, *Sens. Actuators, B*, 2017, **244**, 897–906.

20 L. Zhang, J. Li, C. Wang, J. Tang, X. Chen, Y. Li, J. Shi, P. Zhao, Y. Xie and J. Fei, *Colloids Surf., A*, 2022, **649**, 129484.

21 Q. Tan, C. Chen, C. Lin, J. Zhang, S. Liu and J. Zhang, *Microchem. J.*, 2024, **197**, 109866.

22 J. Sun, Z. Wang and J. Guan, *Food Chem.*, 2023, **425**, 136518.

23 F. Attar, M. G. Shahpar, B. Rasti, M. Sharifi, A. A. Saboury, S. M. Rezayat and M. Falahati, *J. Mol. Liq.*, 2019, **278**, 130–144.

24 P. Ling, S. Cheng, N. Chen, C. Qian and F. Gao, *ACS Appl. Mater. Interfaces*, 2020, **12**, 17185–17192.

25 Md. N. Karim, S. R. Anderson, S. Singh, R. Ramanathan and V. Bansal, *Biosens. Bioelectron.*, 2018, **110**, 8–15.

26 P. Ni, Y. Sun, H. Dai, W. Lu, S. Jiang, Y. Wang, Z. Li and Z. Li, *Sens. Actuators, B*, 2017, **240**, 1314–1320.

27 H. Liu, M. Hassan, X. Bo and L. Guo, *J. Electroanal. Chem.*, 2019, **849**, 113378.

28 S. Shukla, N. N. Joshi, S. Kadian, S. S. Sahoo and R. J. Narayan, *J. Mater. Chem. C*, 2025, **13**, 3886–3901.

29 X. Zhao, Y. Wang, D. S. Li, X. Bu and P. Feng, *Adv. Mater.*, 2018, **30**, 1705189.

30 Y. Chi, W. Yang, Y. Xing, Y. Li, H. Pang and Q. Xu, *Nanoscale*, 2020, **12**, 10685–10692.

31 M. Ataei Kachouei, S. Shahrokhian and M. Ezzati, *Sens. Actuators, B*, 2021, **344**, 130254.

32 B. Liu, Z. Xia, S. Li, W. Hu and C. Lü, *Mater. Today Chem.*, 2024, **41**, 102337.

33 A. Zuliani, M. C. Castillejos and N. Khiar, *Green Chem.*, 2023, **25**, 10596–10610.

34 Y. Liu, X. Zhou, W. Zhu, C. Chen, C. Fan, L. Ding and K. Wang, *Inorg. Chem.*, 2023, **62**, 15022–15030.

35 Ş. Tokalıoğlu, E. Yavuz, S. Demir and Ş. Patat, *Food Chem.*, 2017, **237**, 707–715.

36 X. Y. Song, X. Meng, B. L. Xiao, Y. Y. Li, X. X. Ma, A. A. Moosavi-Movahedi and J. Hong, *Biosensors*, 2022, **12**, 632.

37 H. Beitollahi, F. Movahedifar, S. Tajik and S. Jahani, *Electroanalysis*, 2019, **31**, 1195–1203.

38 Y. F. Gao, T. Yang, X. L. Yang, Y. S. Zhang, B. L. Xiao, J. Hong, N. Sheibani, H. Ghourchian, T. Hong and A. A. Moosavi-Movahedi, *Biosens. Bioelectron.*, 2014, **60**, 30–34.

39 X. J. Fu, C. Meng, L. Guo and L. E. Lin, *Clin. Transl. Oncol.*, 2024, DOI: **10.1007/s12094-024-03684-1**.

40 W. Zhao, Y. Fang, Q. Zhu, K. Wang, M. Liu, X. Huang and J. Shen, *Electrochim. Acta*, 2013, **89**, 278–283.

41 T. Y. Huang, C. W. Kung, Y. T. Liao, S. Y. Kao, M. Cheng, T. H. Chang, J. Henzie, H. R. Alamri, Z. A. Alothman, Y. Yamauchi, K. C. Ho and K. C. W. Wu, *Adv. Sci.*, 2017, **4**, 1700261.

42 S. Biswas, Y. Chen, Y. Xie, X. Sun and Y. Wang, *Anal. Chem.*, 2020, **92**, 4566–4572.

43 K. Zhang, G. Song, Y. Li, X. Wu, K. Li and B. Ye, *Sens. Actuators, B*, 2014, **191**, 673–680.

44 H. Ma, N. Hu and J. F. Rusling, *Langmuir*, 2000, **16**, 4969–4975.

45 P. K. Brahman, N. Pandey, S. N. Topkaya and R. Singhai, *Talanta*, 2015, **134**, 554–559.

46 J. J. Song, Y. Lu, S. W. Zhu, Q. A. Huang and Y. Wei, *Anal. Sci.*, 2015, **31**, 225–230.

47 J. V. Piovesan, C. L. Jost and A. Spinelli, *Sens. Actuators, B*, 2015, **216**, 192–197.

48 Y. Wang, C. Wang, L. Zhang, J. Li, R. Li, Q. Fu, C. Li, P. Zhao, Y. Xie and J. Fei, *Microchem. J.*, 2022, **179**, 107519.

49 M. Chen, K. Umer, B. Li, Z. Li, K. Li, W. Sun and Y. Ding, *J. Colloid Interface Sci.*, 2024, **653**, 380–389.

50 S. Campuzano, M. Pedrero, G. P. Nikoleli, J. M. Pingarrón and D. P. Nikolelis, *Biosens. Bioelectron.*, 2017, **89**, 269–279.

51 F. Mofidi Najjar, F. Taghavi, R. Ghadari, N. Sheibani and A. A. Moosavi-Movahedi, *Arch. Biochem. Biophys.*, 2017, **630**, 81–90.